Developing a site index model for *P. pinaster* stands in NW Spain by combining bi-temporal ALS data and environmental data

Juan Guerra-Hernández [1,2*], Stefano Arellano-Pérez [3], Eduardo González-Ferreiro [4], Adrián Pascual [5], Vicente Sandoval Altelarrea [6], Ana Daría Ruiz-González [3], Juan Gabriel Álvarez-González [3]

[1] 3edata. Centro de iniciativas empresariais. Fundación CEL. O Palomar s/n, 27004 Lugo, Spain. juan.guerra@3edata.es

[2] Forest Research Centre, School of Agriculture, University of Lisbon, Instituto Superior de Agronomia. juanguerra@isa.lisboa.pt

[3] Unidad de Gestión Ambiental y Forestal Sostenible (UXAFORES). Departamento de Ingeniería Agroforestal, Escuela Politécnica Superior de Ingeniería, Universidad de Santiago de Compostela, Campus Universitario s/n, 27002 Lugo, Spain. stefano.arellano@usc.es; anadaria.ruiz@usc.es; juangabriel.alvarez@usc.es

[4] Departamento de Tecnología Minera, Topografía y de Infraestructuras, Grupo de Investigación en Geomática e Ingeniería Cartográfica GI-202-GEOINCA, Escuela Superior y Técnica de Ingenieros de Minas, Universidad de León, Av. de Astorga s/n, Campus de Ponferrada, 24401 Ponferrada, Spain. egonf@unileon.es

[5] Center for Global Discovery and Conservation Science, Arizona State University, Hilo, HA 96720, USA. apascua6@asu.edu

[6] Servicio de Inventario Forestal, Ministerio de Agricultura, Alimentación y Medio Ambiente, 28071 Madrid, Spain. vsandoval@mapa.es

* Correspondence: juan.guerra@3edata.es

Abstract: Site index (SI) is a common measure of forest site productivity, serving as a valuable baseline for forest management. The main objective of this study was to develop a SI model for *Pinus pinaster* Ait. in north-west Spain by combining bi-temporal, low-density airborne laser scanning (ALS) data (acquired in the periods 2009-2011 and 2015-2017) with climatic, edaphic and physiographical data. Site productivity, assessed by site quality curves, was modelled using an age-independent difference equation method based on ALS metrics and environmental variables. For the model development process, we used data from 156 sample plots in pure and even-aged *P. pinaster* stands distributed throughout Galicia (NW Spain) and measured in the Spanish National Forest Inventory (SNFI). The generalized algebraic difference approach (GADA) formulation was tested by using two different base equations for modelling the dominant height growth (ΔH) from ALS variables. The GADA formulation derived from the Bertalanffy's base model produced the best estimates of dominant height (H) for *P. pinaster* stands in Galicia. Use of the proposed model to estimate ΔH for a new pine stand requires two ALS data sets for estimating site-specific (local) parameters. To enable use of the model when such information is not available, the relationship between the values of the site-specific parameter and environmental variables was described using Multivariate Adaptive Regression Splines (MARS). Use of the MARS equation enabled us to develop spatially-explicit predictive maps of the site-specific parameter values, which can be used together with the GADA model to derive ΔH curves and SI estimates for *P. pinaster* stands in the whole study region.

Keywords: LiDAR; Forest productivity; Forest growth modelling; Multi-temporal data

Introduction

Sustainable forest management demands accurate, efficient and up-to-date information in order to describe forest structure and quantify forest productivity (Burkhart and Tomé, 2012). As forest ecosystems are dynamic, it is essential to simulate forest stand attributes projected temporally and spatially to support forest management (Tompalski et al., 2016). Site productivity and forest growth are critical inputs for projecting wood volume and biomass accumulation over time (Skovsgaard and Vanclay, 2008; Diéguez-Aranda et al., 2012). Site productivity, which is commonly determined using site index (SI) models, is also the primary option for many forest management decisions (Álvarez-González et al., 2005; Diéguez-Aranda et al., 2006a, 2009, 2012).

Although SI may not fully represent true site productivity, it is the method most widely used to estimate site productivity for even-aged forests (Álvarez-González et al., 2005; Diéguez-Aranda et al., 2006b). Theoretical growth curves have been developed for estimating SI and predicting dominant height growth (ΔH) of the main productive species in Galicia (for further details, see Diéguez-Aranda et al. (2012). These curves are based on biological relationships and thus give specific meaning to the parameters (e.g. maximum size, growth rate). The curves predict different variables as a function of age, identifying exponential, linear and asymptotic growth stages throughout the lifespan of the tree (Arias-Rodil et al., 2015). However, stand age may not be available for inclusion in growth models. Measurement of this variable can be difficult, as it requires extraction of whole increment cores in tree species with well-defined tree rings (Tomé et al., 2006). The aforementioned study proposed a method for formulating growth functions as age-independent difference equations. Following this approach, Arias-Rodil et al. (2015) concluded that an age-independent equation depending on climatic factors performed best for predicting ΔH, outperforming the traditional age-dependent site quality curves. Recent studies (Scolforo et al., 2019, 2020; González-Rodríguez and Diéguez-Aranda, 2020) indicate the importance of improving the existing growth models by incorporating environmental variables developing site quality maps for different species. Consequently, further research is required to deliver a compatible set of growth equations for prediction and projection. Such equations should include parameters refined by environmental variables to make the empirical models spatially applicable under climate change scenarios.

A number of researchers have pointed out various desirable attributes of dominant height (H) growth models (e.g. Bailey and Clutter, 1974; Clutter et al., 1983; Cieszewski and Bailey, 2000), including the following: (*i*) consistency, i.e. no change for zero elapsed time; (*ii*) path-invariance, whereby the results of projecting the dominant height first from t_0 to t_1, and secondly from t_1 to t_2, must be the same as those of the one-step projection from t_0 to t_2; (*iii*) causality, in which a change in dominant height can only be influenced by inputs within the relevant time interval; (*iv*) polymorphism, i.e. curves for different SI values should not be proportional; (*v*) a sigmoid growth pattern with an inflexion point; (*vi*), horizontal asymptote at old ages, (*vii*) logical behaviour (height should be zero at age zero and equal to SI at the reference age and the curve should never decrease); and (*viii*) theoretical basis or interpretation of model parameters derived by analytically tractable algebraic operations and base-age invariance. Fulfilment of the aforementioned requirements depends on both the construction method and the specific mathematical

function. The algebraic difference approach (ADA) developed by (Bailey and Clutter, 1974), and its generalization, known as GADA (Cieszewski and Bailey, 2000), are useful for this purpose. Numerous studies have used GADA to model the dominant height growth or site index in pine forests in NW Spain (Nunes et al., 2011; Álvarez-González et al., 2005), South of Europe (Bravo-Oviedo et al., 2007, 2008; Kahriman et al., 2018), Central Europe (Socha et al., 2020) and North and South America (Lauer and Kush, 2010; Vargas-Larreta et al., 2013; Scolforo et al., 2016). Dominant height growth (ΔH) equations have the general form (omitting the vector of model parameters) of $Y = f(t, t_0, Y_0)$, where Y is the dominant height at age t, and Y_0 is the reference variable defined as the value of the dominant height at age t_0. The ADA essentially involves replacing a base-model site-specific parameter with its initial-condition solution. The GADA allows expansion of the base equations according to various theories about growth characteristics (e.g. asymptote, growth rate), thereby allowing more than one parameter to be site-specific and allowing derivation of more flexible dynamic equations (see Cieszewski, 2002).

In Spain, the only forest growth information currently available at national and regional scales is that provided by the Spanish National Forest Inventory (SNFI), which began in 1965 (SNFI1). Since the second round of measurements (SNFI2, 1986), the SNFI has been based on a systematic sampling design with permanent plots and previous forest stratification (Spanish Forest Map, SFM) determined by photo-interpretation. It is important to note that the SNFI showcase (Fernández-Landa et al., 2018; Pascual et al., 2020) requires upgrading of the ground positioning protocols to improve data co-registration. Ongoing efforts in this regard (SNFI4 and SNFN, i.e. SNFIs of productive stands in northern Spain) are reducing the gap between nominal and true positions for SNFI samples to allow joint use of the SNFI and remote sensing data for spatial estimation of forest attributes (Pascual et al., 2020).

Airborne laser scanning (ALS) has been a primary source of 3D data on forest vertical structure since the 1990s (Naesset, 1997; Maltamo et al., 2014). An abundance of research has demonstrated the utility of ALS for predicting forest biophysical variables to support forest inventories at individual tree- and stand- level (Hyyppä et al., 2008), providing accurate estimates of tree and stand height (Gatziolis et al., 2010; Guerra-Hernández et al., 2016; Maltamo et al., 2014; Roussel et al., 2017). Multitemporal ALS data have also been used to measure forest height growth, with no statistically significant differences between the field- and ALS-derived mean height increment measurements (Yu et al., 2004, 2006; Hopkinson et al., 2008). A number of recent studies have shown that ALS or image-based

point clouds (obtained by stereo aerial photography) may be valid for estimating SI (Véga and St-Onge, 2008; Tompalski et al., 2015; Socha et al., 2017; Solberg et al., 2019; Noordermeer et al., 2018; 2020; Socha et al., 2020). For instance, Noordermeer et al. (2018, 2020) derived SI based on bi-temporal ALS surveys and existing stand-level models or Solberg et al. (2019) developed an age-independent approach to estimate SI for spruce-dominated stands using repeated single-tree ALS data.

Most studies on ALS and SI have relied on existing height growth models, developed with data collected from permanent sample plots or stem analysis. Calibration of SI models can be replaced by site-specific height growth equations based on growth detected between t_1 and t_2 (the time lapse between ALS surveys), as Socha et al. (2017) reported for Norway spruce forests. The stages of development of commercial tree species are well known, and models based on height dynamics using repeated ALS may therefore be recognized as new, fully valuable wall-to-wall data sources for tree height growth and SI modelling (Socha et al., 2020). In addition, multi-temporal ALS data may also be used for rapid, accurate and cost-effective tree growth assessment, providing up-to-date information to support decision-making in forest management (Hopkinson et al., 2008; Tompalski et al., 2016, 2018, 2019).

The main objective of this study was to predict (ΔH) using an age-independent method based on the GADA approach and data from two ALS acquisitions. The work involved the following: (*i*) comparison of two GADA models based on two well-known base models, to predict and project H and SI in *P. pinaster* stands in Galicia from data acquired in two ALS flights and (*ii*) establishment of a Multivariate Adaptive Regression Splines (MARS) relationship between the site-specific parameter of the GADA model and environmental variables to enable use of the model when data from two ALS flights is not available.

Materials and Methods

Study area

The study area is located in Galicia, in north-west Spain (Fig. 1). This region is characterized by rugged orography and an oceanic climate with mild temperatures, low thermic oscillation between winter and summer and frequent rainfall. The region, which has 1.4 million hectares of tree-covered land and more than 68 million cubic metres of standing timber, provides 51% and 27% of respectively the conifer and total annual harvest volume in Spain (MAGRAMA, 2010). *Pinus pinaster* Ait. is one of the most widely distributed forest tree species in this region, covering an area of more than 276 000 ha (MAPA, 2018).

Field data

The field data used for this study were obtained from the SNFI-4 and SNFI-N. The field measurements of the SNFI-4 in Galicia data were carried out between March and September 2009 (MAGRAMA, 2012), whereas field measurement for the SNFI-N were carried out between May and October 2018 (MAGRAMA, 2018). The SNFI project maintains a network of sample plots throughout the whole country, which are aimed at providing continuously up-dated information on the status of nationwide forest resources, including timber volumes and species composition. Sample plots are established at the intersections of a 1 x 1 km UTM grid and consist of four circular concentric subplots of radius 5, 10, 15 and 25 m. Trees are selected depending on the distance to the plot centre and the diameter at breast height (1.3 m, *dbh*): *i*) trees with $7.5 \leq dbh < 12.5$ cm were measured within a subplot radius of 5 m, *ii*) trees with $12.5 \leq dbh < 22.5$ cm were measured within a subplot radius of 10 m, *iii*) trees with $22.5 \leq dbh < 42.5$ cm were measured within a subplot radius of 15 m and *iv*) trees with a $dbh \geq 42.5$ cm were measured within a subplot radius of 25 m (Álvarez-González et al., 2014; Alberdi et al., 2017). For all trees in the plots, the total height (*h*) was measured with a hypsometer, to the nearest 0.1 m, and the *dbh* was measured in two perpendicular directions with a caliper, to the nearest 0.1 cm. The following stand variables were calculated from the tree variable measurements by using tree expansion factors: number of stems per hectare (*N*), quadratic mean diameter (*dg*), stand basal area (*G*), mean stand height (*h*) and dominant height (*H*, defined as the mean height of the 100 thickest trees per ha). The expansion factor can be defined as the relationship between the reference area (1 ha) and the subplots area adjusting the values of the number of sampled trees to a per hectare value (Álvarez-González et al., 2014)

As stand age is not measured in the SNFI, the site index (SI) of the sample plots cannot be directly estimated from the SI curves developed for the species in the study area. However, an indirect method was used to estimate stand age and SI for SNFI-4 and SNFI-N data. This method requires two measurements of dominant height ($H_{S\text{SNFI-4}}$ and $H_{S\text{SNFI-N}}$) at ages t_1 and $t_1+\Delta t$ for each sample plot, where Δt is the time interval between SNFI-4 and SNFI-N. Using these values, the algebraic difference equation of the SI curves of the species in Galicia (Diéguez-Aranda et al., 2009) can be solved numerically to estimate t_1. Once t_1 is obtained, the same equation can be used to estimate *SI* (m) at a reference age of 20 years, from the values of $H_{S\text{SNFI-4}}$ and t_1.

During field measurement of SNFI-N, the co-registration uncertainty was addressed by using commercial grade global navigation satellite systems (GNSS) to upgrade positioning information on new samples established in forest areas under expansion and on the set of previously existing SNFI-4 sample plots. A handheld data collection system (TRIMBLE Juno 5B handheld, Trimble Inc. USA) was used to determine the coordinates (error range 1-2 m of positioning error after post-processing).

In the first step, all sample plots in which *P. pinaster* predominated (i.e. it represented more than 90% of the trees per ha and more than 90% of total stand basal area in the plot) in both SNFI-4 and SNFI-N were selected. In the second step, exhaustive examination of the data was carried out to reject sample plots with atypical dominant height growth, i.e. values outside the range observed in the *SI* curves of the species in the study area (Dieguez-Aranda et al., 2009); sample plots with lower dominant height and sample plots with dead trees accounted for more than 10% of the basal area. Finally, a total of 156 sample plots of *P. pinaster* were selected for the purposes of the study.

Figure 1 shows the spatial distribution of pure and even-aged *P. pinaster* stands and the selected SNFI sample plots in Galicia. The main stand variables of the SNFI-4 and SNFI-N sample plots used in this study are summarized in Table 1.

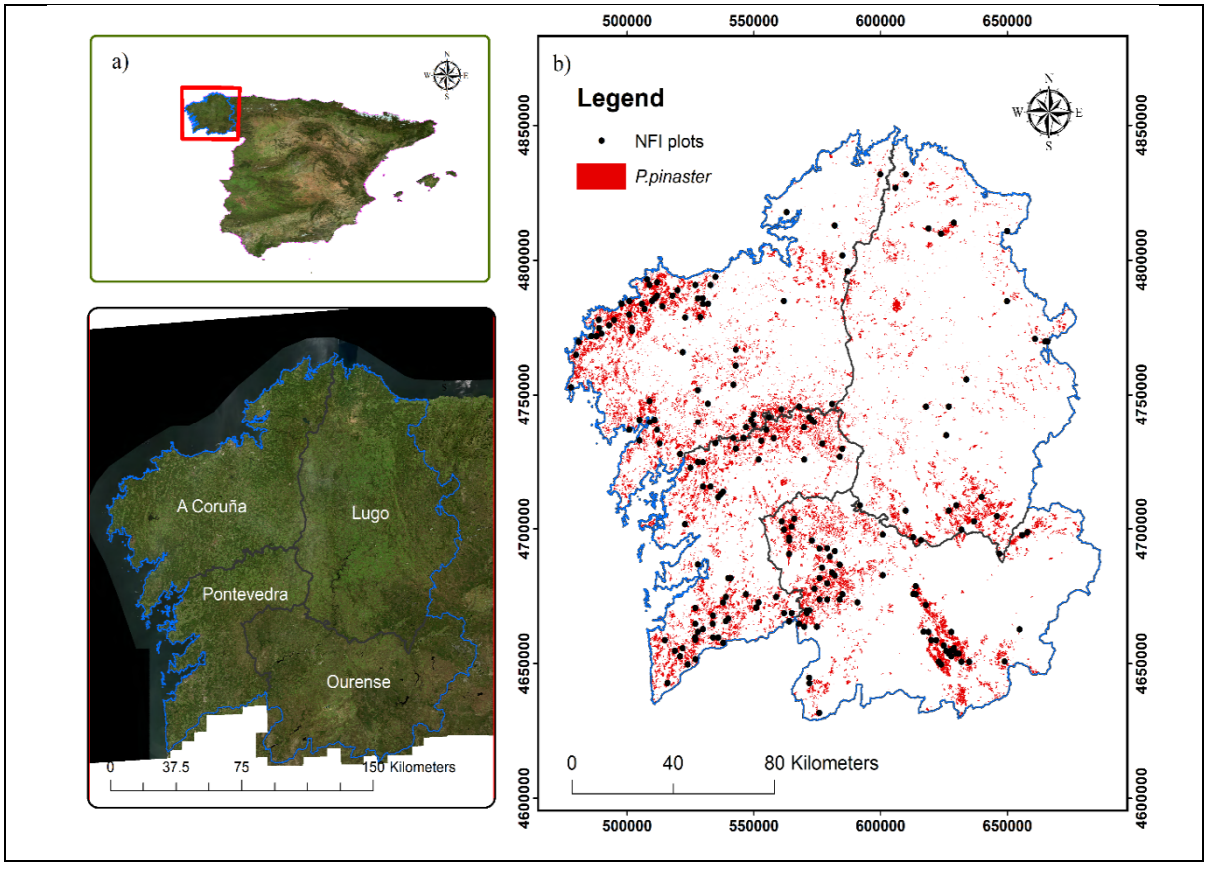

Figure 1. (a) Location of the study area. (b) Spatial distribution of the Spanish SNFI-4 and SNFI-5 plots where *P. pinaster* was dominant (black dots) and the spatial distribution of pure *P. pinaster* (red) stands from latest version of Spanish Forest Map (MAPA, 2018).

Table 1. Summarized statistics of the stand variables observed within 156 field plots.

Inventory	Variable	Mean	Std. dev.	Maximum	Minimum
SNFI-4	*N*	747.85	476.54	2300.46	114.31
	G	28.18	12.19	64.16	8.02
	H	17.47	4.78	28.85	6.33
	V	199.57	112.36	550.15	27.01
SNFI-N	*N*	591.15	374.64	2038.74	110.15
	G	33.62	12.44	80.15	13.52
	H	21.49	4.61	32.62	10.74
	V	273.25	124.32	727.60	37.99
SNFI-4 SNFI-N	*SI*	15.67	5.33	29.81	5.60

where N is the stand density (trees ha^{-1}), G is the stand basal area (m^2 ha^{-1}), H is the dominant height (m), V is the stand volume (m^3 ha^{-1}), and SI is the site index (m), i.e. the value of dominant height at a reference age of 20 years.

ALS acquisition and processing

Two sets of ALS point clouds were processed in this study: the ALS data for the first coverage were collected in the periods September to October 2009 (Galicia East) and February to April 2011 (Galicia West), while the ALS survey in the second coverage took place in the periods July-September 2015 (Galicia West), August-December 2016 and February 2017 (Galicia East). Both data sets correspond to the first and second round of countrywide ALS measurements, which are publicly available in Spain through the National Plan for Aerial Orography (hereafter referred to as PNOA). Square ALS blocks of 2 km side, covering the whole region of Galicia were obtained from the CNIG (Centro Nacional de Información Geográfica) computer server (http://centrodedescargas.cnig.es/CentroDescargas/index.jsp). The scanning sensors involved in collecting the ALS data in the study area were a RIEGL LMS-Q680 for the whole first coverage, and a LEICA ALS50 (West Galicia) and a LEICA ALS80 (East

Galicia) for the second coverage. The nominal laser pulse density varied between 0.5 first returns m^{-2} in the first coverage and 0.5-1 first returns m^{-2} in the second coverage. The vertical accuracy of scanning survey varied between 0.2 and 0.4 m for the first coverage and 0.15 and 0.2 m for the second coverage. The ALS data sets were processed using Lastools software (Isenburg, 2020). A detailed description of the software parametrization and all the processing workflow of ALS point cloud is given by Pascual et al., (2020). Briefly, all ALS echoes classified as ground were used to create a digital elevation model (DEM) considering a spatial resolution of 2 m. The 99th percentile of height distribution was extracted from the normalized ALS point cloud, using a buffer of 25 m of radius from the SNFI-N coordinates of the plot centres (GNSS-based measurements). The above-ground height of ALS echoes was used to distinguish tree canopies (echoes above 2 m) and the shrub layer (echoes below 2 meters) when computing the ALS height statistics (*lascanopy* parameters: height_cutoff = 2, cover_cutoff = 2).

Physiographical, edaphic and climate data

The 2-m resolution DEM was used as the source of physiographical data. At plot level, the ALS ground points were converted to a triangular irregular networks (TIN) surface raster, and 2-m resolution raster using memory-efficient-streaming technology under three parallel processes (Isenburg 2020). The following topographic variables were calculated in R software (R Core Team, 2020), using the *terrain* function in the R *raster* package (Hijmans et al., 2015): elevation, slope, aspect, topographical position index (*TPI*), terrain roughness index (*TRI*) and roughness. Moreover, two trigonometric transformations of azimuth aspect were calculated to characterize the exposure to north-south ($cos\omega$) and east-west effects ($sin\omega$).

The soil variables were obtained from a 500-m resolution raster developed by (Ballabio et al., 2016) for the European territory. These maps provide a set of variables related to soil physical attributes, estimated through interpolation from the soil samples of the LUCAS 2009 TOPSOIL database of the European Soil Data Center (ESDAC) (Panagos et al., 2012). Six soil variables were selected from these raster maps as potential predictors of *SI*: the percentages of sand (%*Sand*), silt (%*Silt*), clay (%*Clay*) and coarse material (%*Coarse*), the soil bulk density (*SBD*, Mg m^{-3}), and the available water capacity (*AWC*), defined as the difference between the field capacity and the water content at permanent wilting point.

Finally, the Digital Climate Atlas for the Iberian Peninsula (Ninyerola et al., 2000, 2007; Pons and Ninyerola, 2008), with 200-m spatial- and monthly temporal- resolution,

267 was used as a source of climate data. The climate variables included in the dataset are
268 average monthly temperature, average maximum and minimum monthly temperature and
269 monthly total precipitation. A set of annual and seasonal climate variables were derived
270 from these original data (http://opengis.uab.es/wms/iberia/). In addition (Table 2), the
271 potential evapotranspiration (*Pe*) was calculated using Thornthwaite´s (1933) equation, and
272 the compensated thermicity index (*Cti*) was obtained using the equation developed by
273 Rivas-Martínez (2008).
274 The descriptive statistics of the physiographical, edaphic and climate variables were
275 extracted from the raster maps for the specific locations of the 156 previously selected
276 sample plots, thus considering its constancy throughout development of each stand. The
277 physiographical, edaphic and climate variables are summarized in Table 2.

278 Table 2. Summary statistics of the physiographical, edaphic and climate variables extracted from the raster datasets corresponding to the 156 sample
279 plot locations.

Variable	Variable	Description	Mean	Std. dev.	Maximum	Minimum
Physiographical	*elevation* (m)	Orthometric elevation	359.26	228.93	912.38	33.88
	slope (%)		12.62	7.35	35.13	0.65
	cosω	North-south effect of azimuth (ω)	-0.03	0.70	1.00	-1.00
	sinω	East-west effect of azimuth (ω)	-0.05	0.71	1.00	-1.00
	TPI (m)	Topographic position index	0.01	0.26	0.85	-1.05
	TRI (m)	Terrain roughness index	1.78	1.10	5.62	0.09
	Roughness (m)		5.77	3.66	17.99	0.55
Edaphic	*%Sand*	Sand textural percentage	55.99	9.25	75.03	30.61
	%Silt	Silt textural percentage	32.28	7.28	52.83	17.56
	%Clay	Clay textural percentage	11.73	2.76	24.63	7.00
	%Coarse	Percentage coarse matter	21.88	6.63	40.17	8.86
	SBD (Mg m^{-3})	Soil bulk density	1.12	0.03	1.16	1.01
	AWC	Available water capacity (soil volume fraction)	0.093	0.006	0.11	0.08
Climate	*T* (ºC)	Mean annual temperature	12.74	1.13	14.99	10.10
	P (mm)	Mean annual precipitation	1280.23	126.53	1529.73	779.58
	Tmax (ºC)	Mean annual maximum temperature	18.04	1.19	20.60	14.90
	Tmin (ºC)	Mean annual minimum temperature	7.451	1.37	9.90	4.70
	Twm (ºC)	Mean temperature of warmest month	19.42	1.20	21.7	15.33

Tcm (ºC)	Mean temperature in the coldest month	7.12	1.43	9.42	3.68
M (ºC)	Mean maximum temperature in the warmest month	25.95	1.88	28.95	19.59
m (ºC)	Mean minimum temperature in the coldest month	2.96	1.48	5.85	-0.61
Ts (ºC)	Mean summer temperature (June, July and August)	18.51	1.65	21.70	13.30
Ps (mm)	Mean summer precipitation (June, July and August)	129.34	24.06	187.54	77.46
Pe (mm)	Potential evapotranspiration (Thornthwaite, 1933)	963.24	123.16	1251.33	706.02
Ci (ºC)	Continentality interval (*Tmax* – *Tmin*)	22.99	2.71	27.41	17.2
Cti (ºC)	Compensated thermicity index (Rivas-Martinez, 2008)	371.64	48.66	464.68	258.63

where $TPI = y - \sum_{i=1}^{8} \frac{y_i}{8}$; $TRI = \sum_{i=1}^{8} \frac{|y_i - y|}{8}$, with y is the altitude of a cell and y_i is the altitude of the i-th adjacent cell; $Pe = \sum_{i=1}^{12} 16 \left(\frac{10T_i}{I}\right)^a$, with $I = \sum_{i=1}^{12} \left(\frac{T_i}{5}\right)^{1.514}$, $a = 0.49 + 0.079 \cdot I - 7.71 \cdot 10^{-5} \cdot I^2 + 6.75 \cdot 10^{-7} \cdot I^3$ and T_i is the mean temperature of the i-th month; $Cti = 10(T + Tmax + Tmin) - 15 \cdot (Ci - 20)$.

Relationship between dominant height and ALS data

In the present study, the *SI* curves were derived using the generalized algebraic difference approach (GADA). The model was developed from the estimates of *H* obtained from the LiDAR metrics of each sample plot and field inventory (SNFI-4 and SNFI-N). For this purpose, a relationship between the *H* field measurements and the LiDAR metrics was previously fitted.

Once the *H* and age values of each sample plot in each field inventory were estimated, the *H* of the sample plots at the time of LIDAR data acquisition was estimated using the site quality curves for this species (Diéguez-Aranda et al., 2009) and the time interval between field measurement dates and flight dates.

Dominant height growth model approach

Two different base equations were evaluated for modelling the ΔH pattern using the GADA approach: Von Bertalanffy, 1957 and Korf, 1939. These functions have been widely used in modelling *H* (e.g., Monserud, 1984; Cieszewski, 2002; Álvarez-González et al., 2005; Diéguez-Aranda et al., 2006a; Castedo-Dorado et al., 2007; Socha et al., 2020).

As general notational convention, a_1, a_2, …, a_n were used to denote the parameters in base models, while b_1, b_2, …, b_m were used for global parameters in subsequent GADA formulations.

The first GADA formulation was tested using the base model proposed by Bertalanffy (1957), the integral form of which can be represented, for the sake of simplicity, as

$$H = a_1\left(1 - exp(-a_2 t)\right)^{a_3} \quad [1]$$

where *t* is the stand age, a_1 is an asymptote or limiting value, a_2 is often called a 'rate parameter', and a_3 is often referred to as 'an initial pattern parameter'. To derive models with both polymorphism and variable asymptotes from Equation (1), more than one parameter must be site specific. Thus, both the asymptote a_1 and the shape parameter a_3 are assumed to be dependent on *X*, a site-specific (local) parameter, using the relationships proposed by Cieszewski (2004):

$a_1 = exp(X)$ and $a_3 = b_2/X$, while $a_2 = b_1$

which defines the following relationship:

$$H = exp(X)\left(1 - exp(-b_1 t)\right)^{b_2/X} \quad [2]$$

Considering two measurements of the same sample plot (t_1, H_1) and (t_2, H_2), both point correspond to the same *SI* curve with the same values of local (*X*) and global parameters (b_1 and b_2):

314 $$\left.\begin{aligned} H_1 &= exp(X)\left(1-exp(-b_1 t_1)\right)^{b_2/X} \\ H_2 &= exp(X)\left(1-exp(-b_1 t_2)\right)^{b_2/X} \end{aligned}\right\}$$

315 Solving t_1 in the first expression and substituting this value in the second one, while
316 considering that $t_2 = t_1 + \Delta$ t, yields:

$$\left.\begin{aligned} H_1 &= exp(X)\left(1-exp(-b_1 t_1)\right)^{b_2/X} \\ H_2 &= exp(X)\left(1-exp(-b_1 t_2)\right)^{b_2/X} \end{aligned}\right\} \Longrightarrow t_1 = -log\left(1-\left(\frac{H_1}{exp(X)}\right)^{X/b_2}\right)\Big/ b_1$$

317 We can then obtain the first GADA formulation [E1] with the general expression $H_2 =$
318 $f(H_1, \Delta t)$ and with two global parameters (b_1 and b_2) and a site-specific (local) parameter
319 (X):

$$H_2 = exp(X)\left(1-exp\left(-b_1\left[\Delta t - log\left(1-\left(\frac{H_1}{exp(X)}\right)^{X/b_2}\right)\Big/ b_1\right]\right)\right)^{b_2/X} \qquad [E1]$$

320 The second GADA formulation is based on the base model proposed by Korf (1939):

$$H = a_1 exp(-a_2 t^{-a_3}) \qquad [3]$$

321 where a_1 is the asymptote parameter, and the other two parameters (a_2 and a_3) are related to
322 the inflexion point and the growth rate. Cieszewski, 2002 replaced a_1 with the exponential
323 of the unobserved site-specific variable X, and a_2 by b_1/X, while $a_3 = b_2$

$$H = exp(X)exp(-(b_1/X)t^{-b_2}) \qquad [4]$$

324 Again, considering two measurements of the same sample plot and solving for t_1 and
325 substituting in the second expression, we obtained the second GADA formulation:

326 $$\left.\begin{aligned} H_1 &= exp(X)exp\left(-(b_1/X)t_1^{-b_2}\right) \\ H_2 &= exp(X)exp\left(-(b_1/X)t_2^{-b_2}\right) \end{aligned}\right\} \Longrightarrow t_1 = \left[-log\left(\frac{H_1}{exp(X)}\right)\left(\frac{X}{b_1}\right)\right]^{-1/b_2}$$

$$H_2 = exp(X)exp\left(-(b_1/X)\left(\Delta t + \left[-log\left(\frac{H_1}{exp(X)}\right)\left(\frac{X}{b_1}\right)\right]^{-1/b_2}\right)^{-b_2}\right) \qquad [E2]$$

327

328 *Dominant height growth model fitting*

329 The GADA models [E1] and [E2] were fitted, by using the SAS/ETS® MODEL
330 procedure (SAS Institute Inc., 2004), to the complete database of sample plots to obtain a
331 single guide-curve with the same global parameters (b_1 and b_2) and a unique estimate of X,
332 common to all sample plots.

333 This guide curve is used as a reference to obtain the specific ΔH curve of a new sample
334 plot (i); for this purpose, the first step consists of estimating the local parameter X_i using
335 [E1] or [E2] with the global parameters of the respective guide-curve and the measurements

of H_1, H_2 and Δt for that specific sample plot, i.e. $X_i = f(b_1, b_2, H_{1i}, H_{2i}, \Delta t_i)$. Once the value of parameter X_i is calculated, the specific curve for the sample plot is obtained using equation [2] or equation [4], with the global parameters of [E1] or [E2], respectively and the local, previously estimated parameter.

In this study, the value of X of each of the sample plots was calculated with the *optimize* function of R (R Core Team, 2020), which uses the method of Brent (1973)) and is appropriate for one-dimensional optimization.

Comparison of the estimates for the two different GADA models was based on numerical and graphical analysis of the residuals (e_{ij}). Two statistical criteria were then examined: the root mean square error (*RMSE*), which analyses the accuracy of the estimates, and the model efficiency (*MEF*), which shows the proportion of the total variance explained by the model, adjusted for the number of model parameters and the number of observations. *MEF* compares predictions directly with observed data using a statistic analogous to adjusted R^2 (Vanclay and Skovsgaard, 1997). This statistic provides a simple index of performance on a relative scale, where 1 indicates a 'perfect' fit and 0 reveals that the model is no better than a simple average. The expressions of these statistics are as follows:

$$RMSE = \sqrt{\frac{\sum_{i=1}^{n}(y_i - \hat{y}_i)^2}{n-p}}$$

$$MEF = 1 - \frac{(n-1)\sum_{i=1}^{n}(y_i - \hat{y}_i)^2}{(n-p)\sum_{i=1}^{n}(y_i - \bar{y})^2}$$

where y_i, $\hat{y}_i$ and $\bar{y}_i$ are the observed, predicted and average values of the dominant height, respectively; n is the total number of observations used to fit the function; and p is the number of model parameters.

Other important steps in evaluating the functions fitted include graphical analysis of the residuals and examination of the appearance of the fitted curves overlaid on the trajectories of the dependent variables for each plot. Visual or graphical inspection is an essential point in selecting the most appropriate model, because curve profiles may differ drastically, even when the fitting statistics and residuals are similar (Huang et al., 2003).

Estimation of the site-specific parameter (X) from physiographical, edaphic and climate data

The GADA models [E1] and [E2] can only be used to obtain the dominant height growth curve of a new sample plot or stand when data from two LiDAR flights are available to estimate the site-specific parameter X ($X_i = f(b_1, b_2, H_{1i}, H_{2i}, \Delta t_i)$). However, from a practical point of view, obtaining this curve from a single flight would be very useful. As parameter X is a specific indicator of productivity because it affects both the asymptote of the site quality curve and its growth pattern, an explicit relationship between this parameter and the site environmental conditions, defined by the physiography, soil and climate variables, was evaluated.

The modelling approaches used should enable development of parsimonious models, preventing overfitting and resulting in relationships where ecological coherence can be easily assessed. In this study, the Multivariate Adaptive Regression Splines (MARS) approach was used to model this relationship. This approach was selected on the basis of the results obtained by González-Rodríguez and Diéguez-Aranda (2020), who evaluated seven different parametric and non-parametric methods for relating the site index of *Pinus radiata* D. Don. stands in the study region (Galicia) to environmental variables, and proposed this method as the most suitable approach.

MARS solution is a nonparametric technique proposed by Friedman, 1991, based on fitting piecewise linear regressions by intervals of the independent variable space. The general form of a MARS model is as follows:

$$y = f_M(x) + \varepsilon \quad [5]$$

where ε is the error, and $f_M(x)$ is the unknown regression function, derived as follows:

$$f_M(x) = \beta_0 + \sum_{i=1}^{M} \beta_i B_i(x) \quad [6]$$

where β_0 is the intercept of the model, $B_i(x)$ are piecewise linear basis functions, β_i is the coefficient of the i^{th} base, and M is the number of base functions. Each piecewise linear base function takes on the following two forms: 1) a hinge function with the form $max(0, x-k)$ with $x-k > 0$ or $max(0, k-x)$ with $k-x > 0$ where k is a constant value called knot; or 2) a product of two or more hinge functions that can therefore model interactions between two or more independent variables (x) defining terms of first, second, third degree, etc.

The optimal MARS model is determined in a two-stage process. First, MARS constructs a very large number of base functions that fit the data with different degrees of accuracy. Second, the generalized cross-validation (GCV) criterion is used and the set of base functions with the lowest value of GCV is selected:

$$\mathrm{GCV(M)} = \frac{\sum_{i=1}^{n}(y_i - f_M(x_i))^2}{n\left(1 - \frac{p_M}{n}\right)^2} \quad [7]$$

where y_i represents the observed values of dominant height, n is the number of sample plots and p_M is the number of model parameters. The MARS model was fitted with the earth package (Milborrow et al., 2019) implemented in R software (R Core Team, 2020).

The use of these large-scale models outside the range of values of the sample used to develop them could result in abnormal estimates of the local parameter *X*, which would produce unusual site index and dominant height growth values. To avoid this drawback, some restrictions have been established for the maximum and minimum estimates of this parameter *X*. In a comprehensive assessment of the site quality of the species in the study area, the minimum and maximum *SI* values derived from stem analysis of 204 dominant trees were respectively 6.7 and 21.9 m (Álvarez-González et al., 2005). Therefore the extreme estimates of the *X* parameter will be those leading to these maximum and minimum of the site index.

Results

Relationship between dominant height and ALS data

The Pearson's correlation coefficients were computed for *H* field measurements and the ALS percentiles. The highest value was obtained for the 99th percentile, and a linear relationship for estimating *H* from h_{p99} was thus fitted using the previously estimated values of *H* for the 156 sample plots at the time of both LiDAR acquisitions. The model explained more than 89% of the observed variability (Figure 2). Finally, the fitted relationship was used to estimate the dominant heights of each sample plot for the two LiDAR acquisition dates.

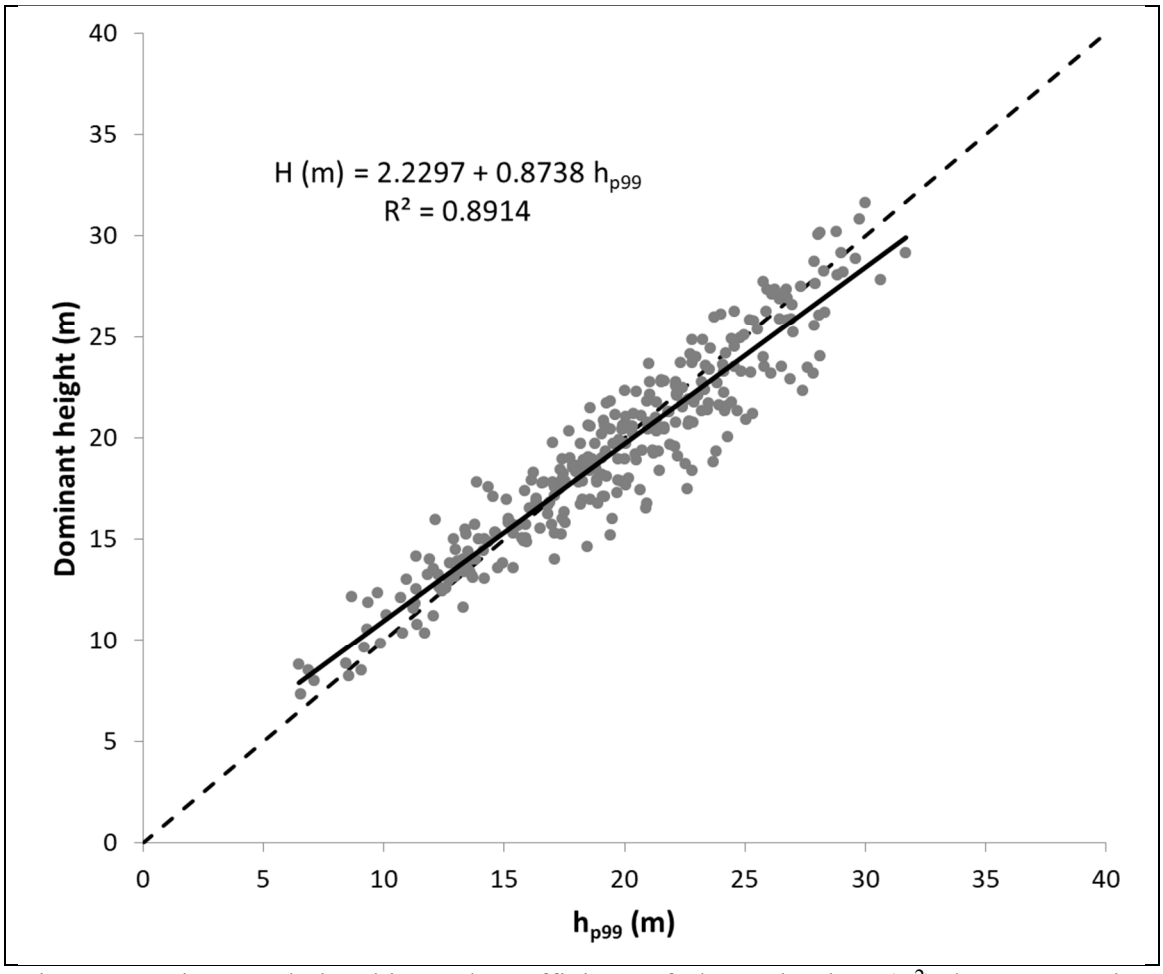

Figure 2. Linear relationship and coefficient of determination (R^2) between estimated dominant height at the time of both LiDAR acquisitions (H, m) and the 99th percentile heights from the distribution of ALS echoes.

Dominant height growth model

The parameter estimates for both GADA equations [E1] and [E2], the approximate standard errors and the corresponding goodness-of-fit statistics are shown in Table 3. Both GADA equations produced very similar values for the goodness-of-fit statistics, explaining more than 91% of the total observed variability in height increment. In addition, the distribution of residuals against the estimated values is also very similar in both models (Figure 3). For a more detailed comparison between the models, the mean annual increment (MAI) in dominant height in each plot has been estimated for each model (E[1] and E[2]) and compared with the field-observed values for different age classes and site indexes (Figure 4).

434 Table 3. Parameter estimates and goodness-of-fit statistics for the GADA equations fitted to
435 model dominant height growth using two different base-models: Von Bertalanffy (1957)
436 [E1] and Korf (1939) [E2].

Model	Parameter	Estimate	Approx. SE	RMSE(m)	MEF
	b_1	0.01829	0.0059		
E1	b_2	2.7972	1.0629	1.2366	0.9128
	X	3.6997	0.2847		
	b_1	33.1988	4.2729		
E2	b_2	0.4995	0.0612	1.2367	0.9128
	X	4.3487	1.3047		

437 where, *b1, b2* = global parameters, X = site-specific parameter

438

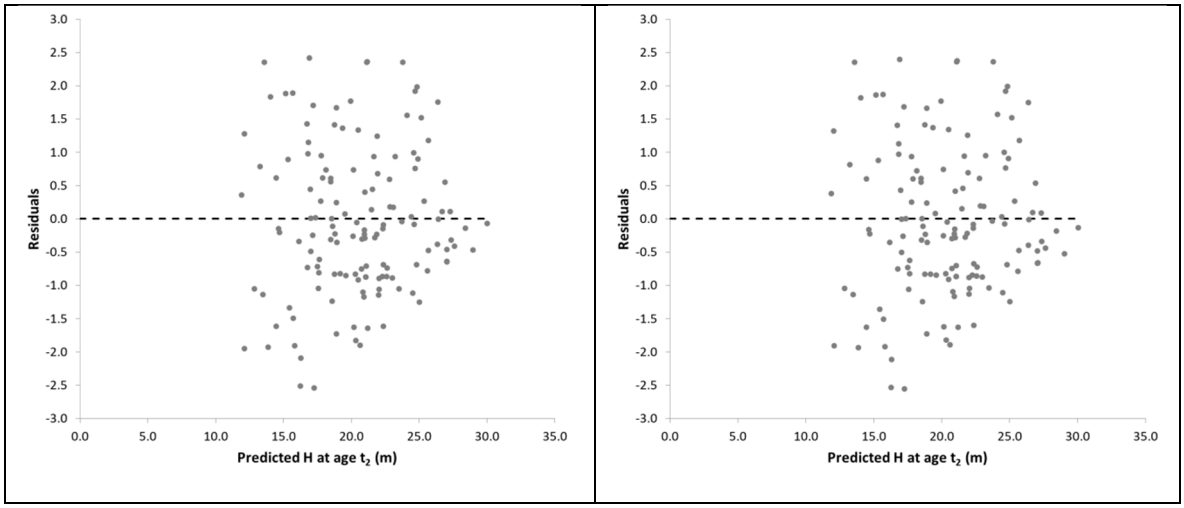

439 Figure 3. Plot of residuals versus predicted dominant height at age t_2 from model E1 (left)
440 and E2 (right)

441

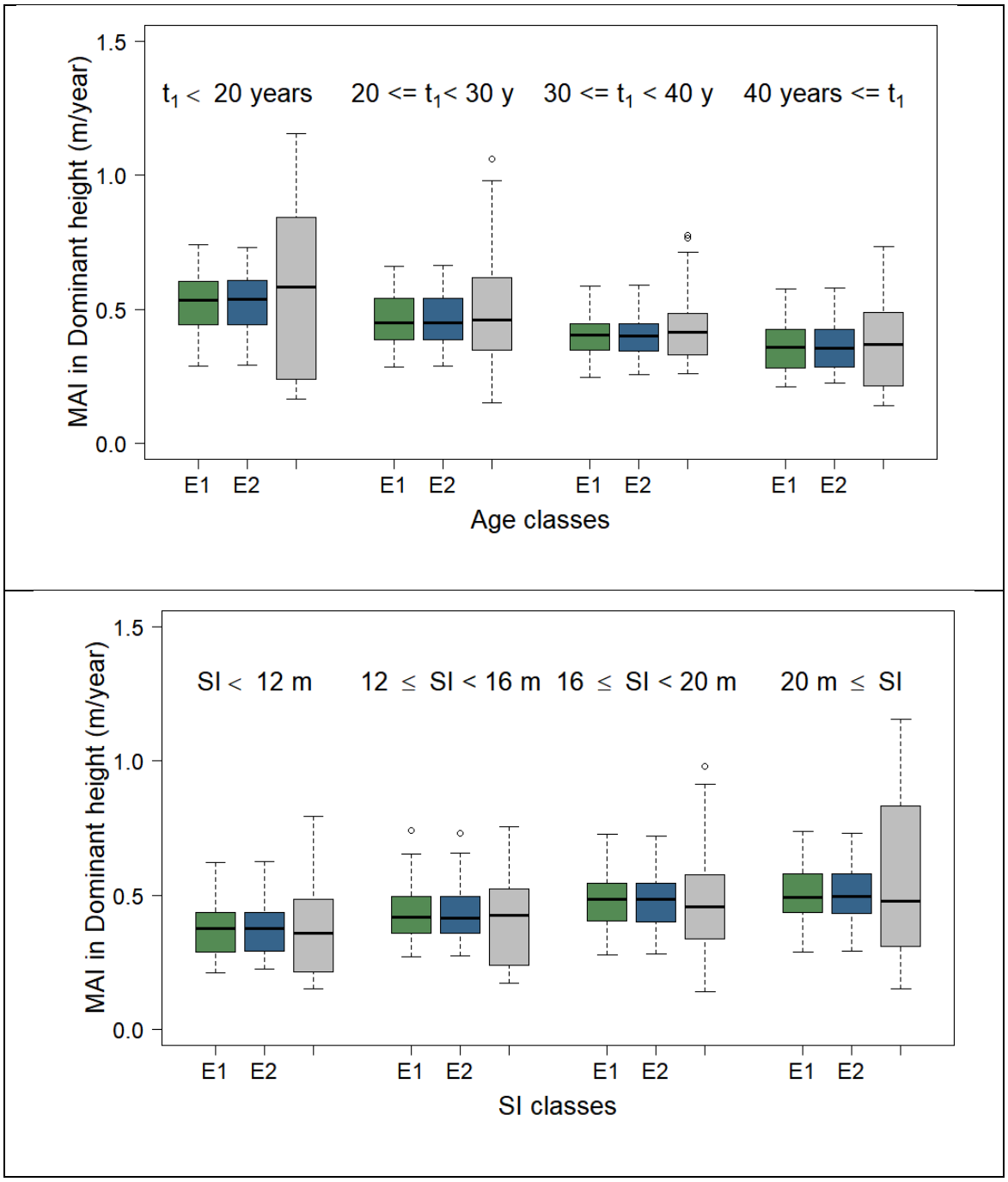

442 Figure 4. Boxplots of mean annual increments (MAI) in dominant height obtained with
443 each model ([E1] and [E2]) and field-observed values (grey colour) of the sample plots for
444 different age (upper) and site index classes (lower).
445
446 As shown in Figure 4, there are no perceptible differences between the results obtained
447 with both GADA equations analysed, so finally, to select the best model, a set of curves
448 corresponding to *SI*s of 8, 13, 18, 23 and 28 m at a reference age of 20 years was obtained
449 for each GADA equation and overlaid on the trajectories of the *H* of each sample plot for a
450 graphical analysis (Figure 5).

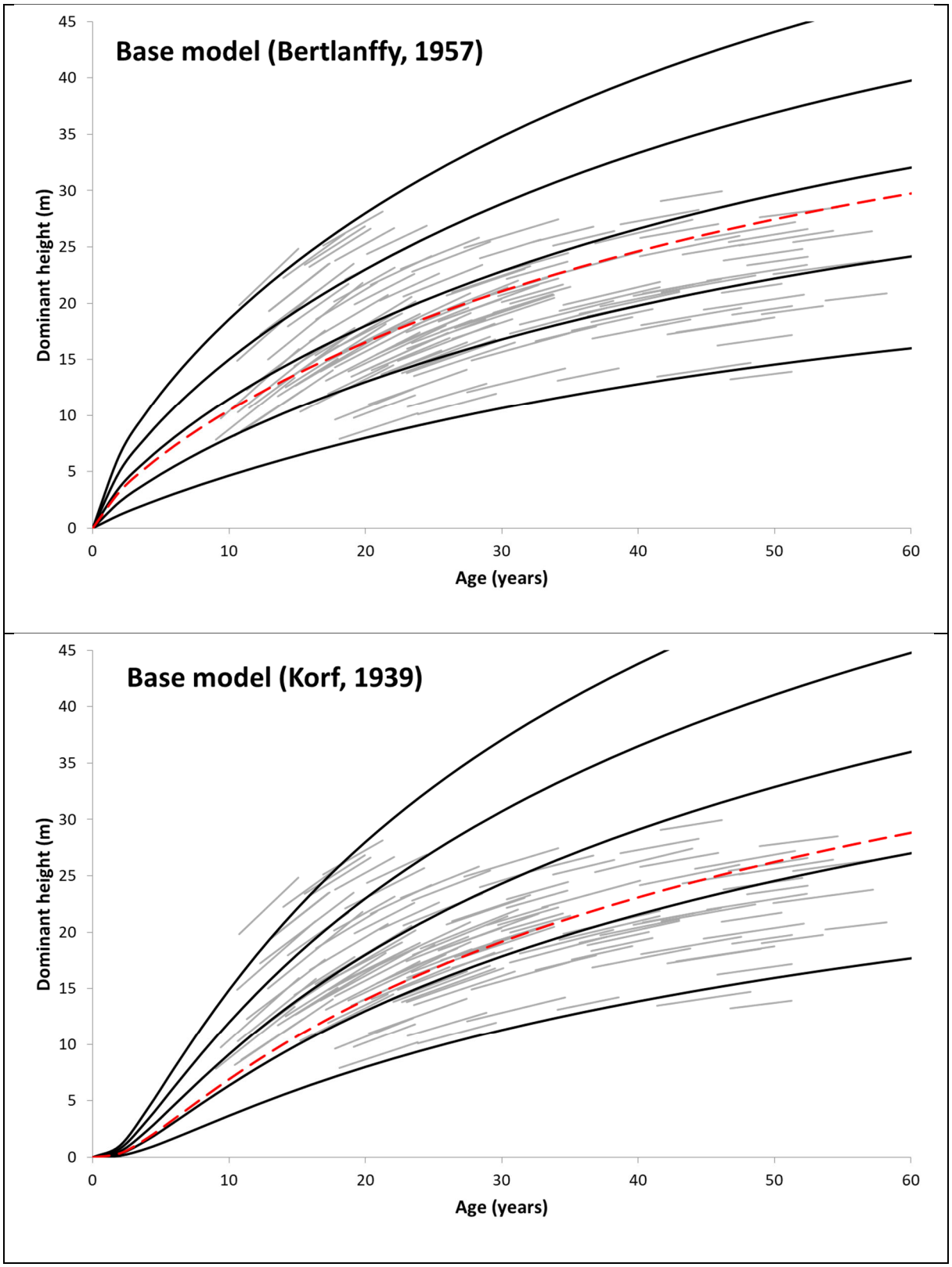

451 Figure 5. Height development curves (black lines) for site indices of 8, 13, 18, 23 and 28 m
452 at a reference age of 20 years, derived from equation [E1] (upper) and equation [E2]
453 (lower), overlaid on the trajectories of dominant height (grey lines) estimated for each
454 sample plot from the 99th height percentile from ALS data in 2009-2011 and 2015-2017.
455

Graphical inspection indicated that model [E1] slightly underestimate the growth rate for young stands ranging from 10 to 20 years old, whereas model [E2] derived from the base model proposed by Korf (1939), overestimated height growth for the best site qualities, and the curves generated from this model seemed to increase more quickly than the trajectories of sample plots. Overall, although both models have a very similar behaviour, based on the superimposition of the site quality curves on the observed trends of the plots, the age-independent equation [E1], derived from the Bertalanffy's (1957) base model, was proposed for modelling dominant height growth for *P. pinaster* stands in Galicia:

$$H_2 = e^X \left(1 - exp\left(-0.01829\left[\Delta t - log\left(1 - \left(\frac{H_1}{e^X}\right)^{X/2.7972}\right)/0.01829\right]\right)\right)^{2.7972/X} \quad [8]$$

where H_1 and H_2 are the dominant heights estimated using data from two ALS flight surveys carried out for a time interval Δt, and X is the site-specific (local) parameter to be estimated.

Once parameter X was obtained for a sample plot, the specific curve for that sample plot can be obtained using the original base model equation with the global parameters (equation [9]). The *SI* of the sample plot will be the dominant height estimated using the specific equation for a reference age of 20 years (equation [10]):

$$H = exp(X)\left(1 - exp(-0.01829t)\right)^{2.7972/X} \quad [9]$$

$$SI = exp(X)\left(1 - exp(-0.01829 \cdot 20)\right)^{2.7972/X} \quad [10]$$

where H is the predicted dominant height (m) at age t (years), *SI* is the site index (m) and X is the site-specific (local) parameter.

The values of X parameter can be obtained from equation [8] using two dominant heights (H_1 and H_2) estimated using data from two ALS flight surveys carried out for a time interval Δt:

$$H_2 - e^X \left(1 - exp\left(-0.01829\left[\Delta t - log\left(1 - \left(\frac{H_1}{e^X}\right)^{X/2.7972}\right)/0.01829\right]\right)\right)^{2.7972/X} = 0$$

As discussed previously, it is necessary to restrict the estimates of parameter X obtained from the above equation to avoid unusual values. Solving equation [10] for parameter X using the range of *SI* observed for the species in the study area (6.7 and 29.1 m; Álvarez-González et al., 2004) yielded estimates of 3.0037 and 4.1652. Therefore, a

minimum value of 3 and a maximum value of 4.1 were assumed for the site-specific parameter.

Site-specific parameter model

The value of the site-specific parameter *X* required for practical use of equations 9 and 10 has some restrictions as it affects both the value of the asymptote and the growth pattern of the curves generated with the GADA model. Taking into account a minimum value of 3 assumed for this parameter, the following model formulation was selected to guarantee fulfilment of this limitation:

$$X = 3 * \left(1 + exp(\alpha_0 + \alpha_i Y_i)\right) \quad [11]$$

where Y_i is a set of environmental variables and α_0, α_i are parameters to be estimated.

Equation [11] was log-linearized ($log(X/3 - 1) = \alpha_0 + \alpha_i Y_i$), and the MARS model was fitted to the values of the new dependent variable.

The best results in terms of the generalized cross-validation (GCV) criterion was obtained with a total of 14 basis functions (intercept, 5 first degree basis functions and 8 second degree basis functions) including 13 environmental variables. The expression for the basis functions is shown in Table 4.

Table 4. Parameter estimates and basis function of the MARS model fitted to estimate the site-specific parameter *X* from environmental variables.

Parameter	Estimate	Basis function
α_0	-1.1774	
α_1	1.7070	(6.0695-*Tmin*)
α_2	-0.0675	(*%Clay*-13.8485)
α_3	-5.9814	(*SBD*-1.0824)
α_4	-0.0155	(*altitude*-533.5570)
α_5	-0.0161	(869.2190-*Pe*)
α_6	0.0001	(*altitude*-533.557)·*Ps*
α_7	0.0112	(*Tmin*-6.0695)·(15.9403-*slope*)
α_8	0.0171	(*Tmin*-6.0695)·(884.5470-*Pe*)
α_9	-0.0001	(30.2877-*%Silt*)·(533.557-*altitude*)
α_{10}	0.0437	(*SBD*-1.1251)·(533.557-*altitude*)
α_{11}	-0.1129	(2.2205-*TRI*)·(0.6824-*sinω*)

α_{12}	-0.0992	(0.1424-*TPI*)·(*Roughness*-6.7759)
α_{13}	-0.0019	(19.8899-*Twm*)·(*Pe*-869.2190)

501

502 The parameters and the basis functions of the MARS fitted model were substituted in
503 equation [11], and the *X* estimates obtained with this transformed model explained 57.69%
504 of the observed variability in the site-specific parameter, with a GCV value of 0.0229.

505 The importance of each environmental variable included in the MARS model was
506 evaluated in terms of the decrease in the residual sum of squares of the model due to its
507 inclusion, and the results were scaled so that the variable yielding the largest summed
508 decrease is assigned a value of 100. Figure 6 shows the scaled importance of the
509 environmental variables included in the MARS model.

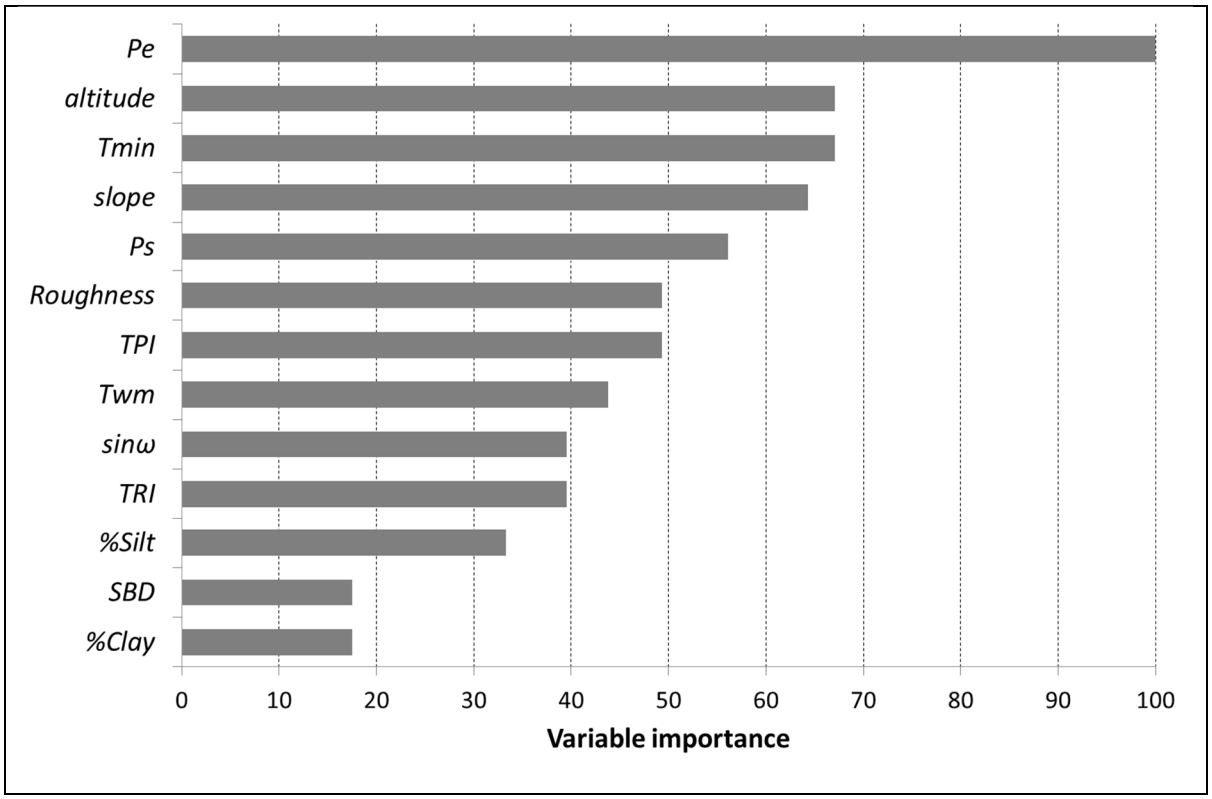

510 Figure 6. Scaled importance of the environmental variables included in the MARS model in
511 terms of residual sum of square reduction (the variables are described in Table 2)

512

513 To assess the performance of the MARS model fitted, four different plots were
514 analysed. In a first step, the accuracy of estimates of the MARS model was evaluated by
515 analysing the plots of site-specific parameter observed versus site-specific parameter
516 estimated with the model (Figure 7a) and residuals versus predicted values of the site-
517 specific parameter obtained with the model (Figure 7b). Finally, the *X* estimates were used

518 to obtain the *SI* of each sample plot using equation [10] and plots of observed versus
519 predicted *SI* (Figure 7c) and residuals versus predicted *SI* (Figure 7d) were analysed.
520 .

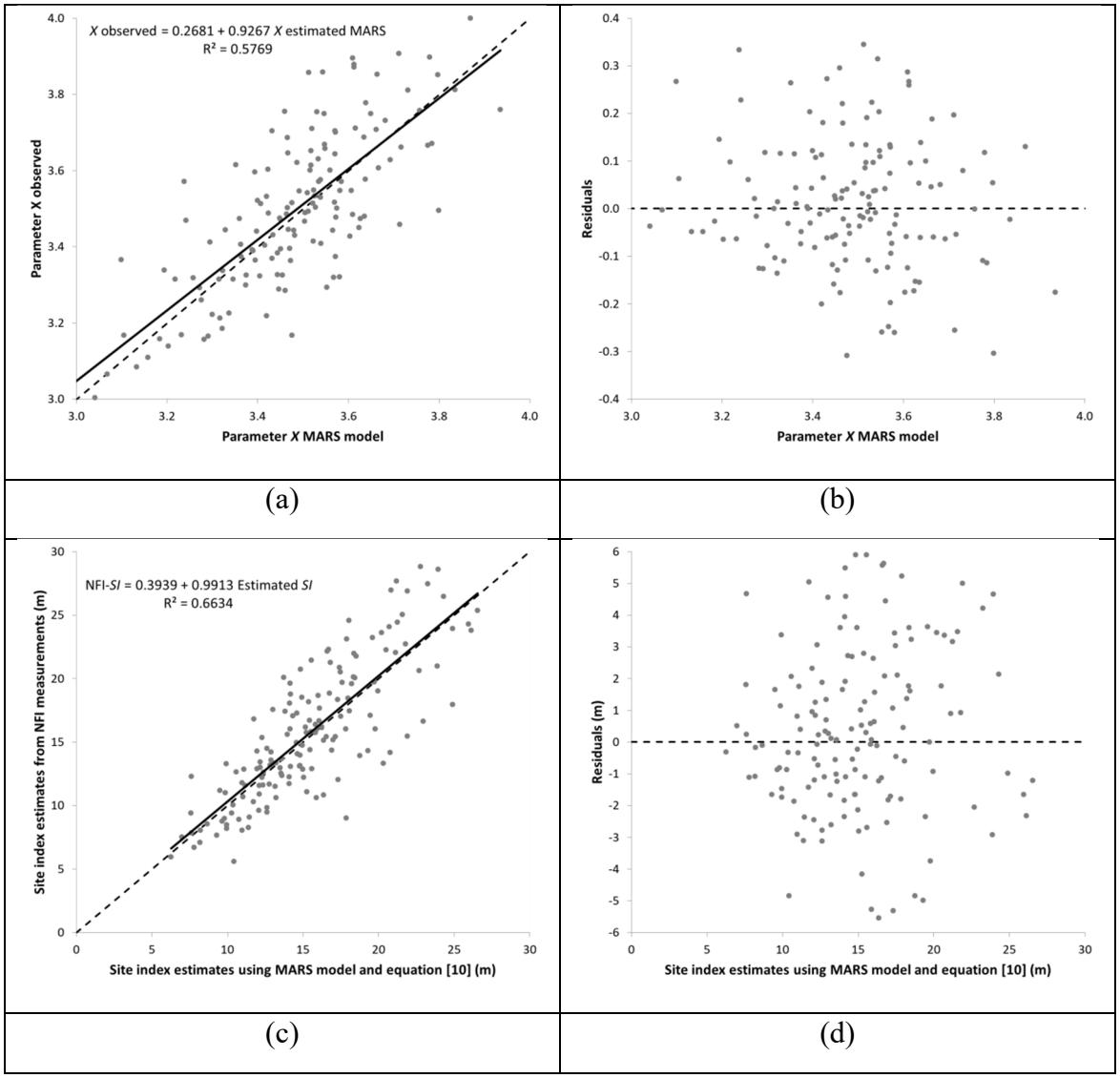

521

522 Figure 7. Scatter plot of: a) observed site-specific *X* parameter versus site-specific *X*
523 parameter estimated using the MARS model; b) residuals versus predicted values of local
524 parameter (*X*) estimated with the MARS model; c) observed *SI* values versus predicted *SI*
525 values using the MARS model to estimate the *X* parameter and then equation [10]; d)
526 residuals versus predicted values of *SI* estimated using the MARS model and then equation
527 [10] (d). The solid line represents the fitted linear model.
528

Discussion

Galicia is one of the most important regions in Spain in terms of forestry production (69% of the land is covered by forest), and pure *P. pinaster* stands, the most extensive forest type in Galicia until the end of the 20th century, still represent more than 15% of the Galician forests, i.e. they are the second most abundant productive forests in Galicia (MAPA, 2018). Obtaining further knowledge about forest ecosystems could improve forest management and decision-making for improved productivity and competitiveness of the forestry sector in Galicia.

The present study demonstrates the potential of bi-temporal ALS data, which when combined with other sources of freely available environmental data enabled us to develop regional *SI* models for *P. pinaster* stands in Galicia. The multitemporal low-density ALS data from the PNOA (with a planned temporal resolution of 6 years) is promising auxiliary data for improving traditional *SI* modelling, while spatially capturing changes across forest landscapes. The method developed, which combines two ALS surveys and the SNFI ground data sets, enables shifts from age-dependent to age-independent *SI* models, while respecting the underlying principles of *SI* modelling (see Introduction). Thus, the age-independent models presented boost the capacity of ALS to account for changes over time without any constraints to age measurement. Noordermeer et al. (2020) and Socha et al. (2019, 2020) recently highlighted the potential of multitemporal ALS data observations for modelling *SI*. The proposed methods could be applied to mapping local site-specific *SI* models, to address the problem of uncertainty in forest growth estimation due to local variation and also to improve large-scale forest productivity estimation in regions such as Galicia.

The base models used to develop the GADA equations [E1] and [E2] have been widely used to develop age-dependent site index curves. For example, Betarlanffy´s base model was selected in the studies by Scolforo et al. (2016), for eucalypt plantations in Brazil, and by Seki and Sakici (2017), for Crimean pine in Turkey, whereas Korf's base model proved more accurate for even-aged natural longleaf pine in US (Lauer and Kush, 2010) and for Calabrian pine in Turkey (Kahriman et al., 2018) than Bertalanffy's base model. Although both GADA equations [E1] and [E2] are quite flexible and proved equally accurate for estimating dominant height, an ideal solution was not achieved since [E1] model tended to underestimate the height growth for young stands and [E2] model tended to overestimate for high qualities. Nonetheless, it is usually recommended to apply with caution the site

quality curves to young stands due to possible errors in dominant height growth estimates and site indices (e.g. Weiskittel et al., 2011), so we considered that the behaviour of the [E1] model, derived from the Bertalanffy's (1957) base model, was the most appropriate to model the growth in dominant height.

The selected GADA equation to estimate the height growth curves using multitemporal ALS data explained more than 91% of dominant height growth variability. This value is lower than that reported by Socha et al. (2020), which explained the 99% of the observed variability using a 99th percentile, 30-m resolution layer for Scots pine in Poland. However, the model developed in the present study is age-independent, while that developed by Socha et al. (2020) is age-dependent, so that the comparison is not conclusive.

A key factor in the development and practical use of the fitted GADA model is an accurate estimation of the dominant height from LiDAR metrics. The adjusted linear relationship in this study explains just over 89% of the observed variability using the 99th percentile as the only independent variable (Figure 2). This result contrasts with that obtained by Socha et al. (2020) in a study on the effect of different LiDAR metrics on site index model estimates. These authors observed that the use of the 99th percentile tended to underestimate the growth in dominant height, especially in older stands with a reduced number of trees and broken crown closures, and recommended the use of the 100th percentile or the estimation of the dominant height by using individual tree detection. Although the model obtained in this study based on the 99th percentile has a slight bias (-0.23 m), the use of the 100th percentile resulted in more biased (-1.33 m) and less accurate estimates (RMSE increased from 1.74 to 2.50 m). One of the possible reasons for this difference could be the definition of dominant height used in each case, the mean height of the 100 thickest trees per hectare in our case and that proposed by Rennolls (1978) in Socha et al. (2020). Another factor that could cause these contradictory results is the high density of *Pinus pinaster* stands in the study area with a mean value of 669 trees ha^{-1}, so the situations where Socha et al. (2020) found higher underestimates (low-density stands with open coverages) are not so frequent. In addition, another factor possibly influencing the results is the low density of the ALS data in our study (0.5-1 pulses m^{-2}) compared with that used by Socha et al. (2020) (7-10 pulses m^{-2}).

Pulse density is widely recognized to be one of the most important factors influencing the accurate estimation of tree height from ALS (Hyyppä et al., 2008; Roussel et al., 2017). It has been established that LiDAR systems tend to underestimate tree height (Hyyppä et al. 2008), which is consequence of the operation of the scanner and the inadequate

representation of canopy apices due to low point density (e.g. Gonçalves-Seco et al., 2011; Roussel et al., 2017). Laser pulse density and vegetation structure are also important issues in relation to the height accuracy of the laser-derived Digital Elevation Model (DEM) to normalize the height (Clark et al., 2004; Raber et al., 2002; Valbuena et al., 2011), especially on steep terrain (Estornell et al., 2011). Therefore, the determination of the height increment working with a low-density point cloud, especially in the short term interval, could be subject to a large error (Hopkinson et al., 2008). According to Hopkinson et al. (2008), the ALS observation interval in our study was considered enough to capture height growth trend without large errors. These authors, in a study of height growth in red pine conifer plantations using low-density ALS data, reported that both the absolute and relative magnitudes of plot-level uncertainty decrease in a power–function relationship with the annual time increment, such that after three years the level of uncertainty in the LiDAR growth estimate rapidly drops to an operationally acceptable level of approximately 10%; with additional time providing minimal increases in accuracy (Hopkinson et al., 2008). This is shorter than a typical five-year time interval of field-based repeat height assessment for similar conifer plantations.

Another limitation of the proposed approach is that two ALS flights are needed to produce the ΔH curve of a new sample plot or stand to estimate the site-specific parameter (X). Thus, a compatible model for predicting and projecting height growth and including a MARS equation to estimate the site-specific local parameter X from environmental variables was developed for the species in the study region. The fitted MARS equation explained more than 57% of the total variation in the observed site-specific parameter based on physiographical, edaphic and climate variables (Figure 7a). Moreover, the site indices obtained from estimates of parameter X using equation [10] explained more than 66% of the observed variability in site indices derived from field measurements (Figure 7c).

According to the results of the variable importance analysis (Figure 6), the geomorphometric variable (*elevation*) and potential evapotranspiration (*Pe*) were the most important predictors for describing the relationship between site-specific parameters and environmental variables. These results also suggest that the physiographical variables extracted from DEMs may be just as important or more important than edaphic and climatic variables for characterizing the potential production of *P. pinaster* in the study area, as in addition to *elevation*, the variables *slope, TPI* and *Roughness* were among the subsequently most important variables for site-specific parameter modelling. This is consistent with the findings of Rodríguez-Soalleiro (1995) and Álvarez-Álvarez et al. (2011), who used

630 elevation as a significant variable for *P. pinaster SI* modelling in Galicia and Asturias,
631 respectively. *TRI* and *sinω* were also included among the 13 significant environmental
632 variables in the MARS model, highlighting the importance of small-scale orographic
633 effects in Galicia. It is important to note that *slope*, *TRI, sinω* were also included as
634 physiographic predictors in the MARS model developed by González-Rodríguez and
635 Diéguez-Aranda (2020) to estimate the *SI* of *P. radiata* plantations, which used 13
636 environmental variables and a 200-m resolution DEM for a regional study in Galicia.
637 Four climatic variables were also included in the fitted MARS equation: more
638 specifically, *Pe* (Potential evapotranspiration), *Tmin* (mean annual minimum temperature)
639 and *Ps* (Mean precipitation in summer) were among the 5 most important variables
640 explaining the variation in the site-specific parameter *X*. Similar results have been obtained
641 for the same species in the neighbouring region of Asturias (NW Spain) (Álvarez-Álvarez
642 et al. (2011) and Arias-Rodil et al. (2015)). The first researchers evaluated the effects of
643 foliar nutrients and environmental factors on site quality of *P. pinaster* stands in Asturias,
644 observing that *SI* was higher in stands with a higher mean summer temperature (*Ts* in ºC)
645 and lower winter precipitation (*Pw*, in ºC). By contrast, Arias-Rodil et al., (2015) fitted
646 different linear relationships to relate a site-specific parameter of a dominant height growth
647 model and environmental variables, obtaining the best results with minimum mean
648 temperature of the coldest month (*Tcm*) and mean annual precipitation (*P*) as independent
649 variables. The models developed for Asturias (Álvarez-Álvarez et al., 2011; Arias-Rodil et
650 al., 2015) were based on sample plot grids established in a pure Atlantic climate in the area
651 of distribution of *P. pinaster*, while the sample plots used in this study were spread along
652 areas characterized by Atlantic, continental and even Mediterranean climate conditions,
653 which may explain the relative importance of *Ps* and *Tmin*.
654 In the present study, *Pe* was the most important variable in the MARS model in
655 terms of reduction of the residual sum of squares. Numerous previous studies have reported
656 the influence of *Pe* on forest growth (e.g. Kimmins et al., 1990; Wickramasinghe, 1988;
657 Martínez-Vilalta et al., 2008; Liu and El-Kassaby, 2018). This variable is closely related to
658 water deficit (Gracia et al., 1999) and worsening of drought conditions (Klos et al., 2009;
659 Scolforo et al., 2013; Vicente-Serrano et al., 2014; Gazol et al., 2017; Gleason et al., 2017),
660 both of which can constrain forest growth. In agreement with other studies in eucalyptus
661 and pine stands in Brazil (Scolforo et al., 2013; Campoe et al., 2016; Scolforo et al., 2020),
662 our findings suggest that the inclusion of *Pe* as predictor could integrate the effect of
663 physiographical, soil and climate variables in dominant height growth modelling, thereby

664 increasing the ability of the model to estimate site quality. The *SI* model proposed by
665 Scolforo et al. (2020) included mean annual soil water deficit (mm $year^{-1}$), which used the
666 monthly differences between potential and actual evapotranspiration, calculated by the
667 water balance model of Thornthwaite-Mather. Campoe et al. (2016) found that *Pe*, along
668 with other variables such as maximum temperature and vapour deficit, were related to the
669 annual increase in tree basal area in pine and eucalyptus plantations in Brazil. Bravo-
670 Oviedo et al. (2008) indicated that drought length, mean annual temperature, and
671 precipitation regimes prior to the growth season (total autumn and winter precipitation)
672 were considered regional differentiation factors to explain differences in the dominant
673 growth pattern of *P. pinaster* stands for four different regions in Spain. Finally, Condés and
674 García-Robredo (2012) reported the influence of precipitation, temperature, Emberger
675 index and free climatic intensity (the latter dependent on *Pe*) on the stand volume growth in
676 *P. halepensis* stands in SE Spain.
677 The edaphic variables silt (%*Silt*), clay (%*Clay*) and soil bulk density (*SBD*,
678 Mg m^{-3}), which are related to soil water capacity, were the most important edaphic drivers
679 explaining *P. pinaster* height growth. However, the strictly edaphic variables were the least
680 important from the point of view of reducing the residual sum of squares in the MARS
681 model. This is also consistent with previous findings of Arias-Rodil et al. (2015), who
682 reported that *SI* models including a third variable related to soil characteristics explained
683 only 1–2 % more variability than models including only climate variables.
684 We developed a two-equation system to predict ΔH and *SI*, which represents an
685 advancement towards improving forest management decisions for *P. pinaster* stands in
686 Galicia and identifying remotely sensed features that enable reliable estimation of ΔH and
687 SI. The system is flexible, and it supports forest management planning, maximizing the use
688 of ALS surveys and ground data from SNFIs. The value added by this research is related to
689 the opportunity to generate *SI* models for application at several spatial scales, for a wide
690 geographic distribution of the forest species at regional level and supporting the change in
691 paradigm in the field of forest growth and site quality (age independency).
692 With the rapid development of forestry-oriented enterprise consultancies and the
693 solid progress of the PNOA-LiDAR project, ALS surveying is becoming a multi-purpose
694 tool in Spain. In addition, new accurate positioning of SNFI plots (GNSS-based) will
695 contribute greatly to improving large-scale estimates of biophysical forest attributes
696 (Guerra-Hernández et al., 2016, 2019). For instance, the models presented here can be used
697 for automatic mapping of *SI* over large areas of *P. pinaster* stands, representing forest

productivity, which may be of interest for inclusion in the Spanish Forest Map (SFM). The first countrywide ALS coverage is already available for the whole Spanish territory, and the second countrywide ALS coverage will soon be available for all Spanish regions, with the theoretical average point density data ranging from 0.5 to 14 points m^{-2}. Therefore, in the near future, the amount of data available from ALS surveys will increase the importance of change detection by ALS in forest growth modelling (Yu et al., 2006; Hopkinson et al., 2008; Socha et al., 2017). Finally, Ice-Sat2 and GEDI NASA´s missions could also improve forest productivity modelling by increasing the availability of data in real time and decreasing the temporal resolution. For future improvement of cartography, better resolution of edaphic and climate rasters should also be considered for assessing *SI* and forest growth by using environmental variables.

Conclusions

SNFI data and multitemporal low density ALS data from the PNOA were used to develop a regional site index model for *P. pinaster* stands in Galicia. A two-equations system comprising one equation from two ALS flights and a complementary equation including environmental variables as predictors (for when only one ALS flight is available) is proposed. Consequently, site quality maps for the whole region could easily be developed by combining the age-independent GADA model proposed, information from any future ALS flight surveys and cartography of the distribution of the species in Galicia. The MARS model developed in order to estimate the site-specific parameter of the GADA model from environmental variables performed well, with a relatively robust and parsimonious form (13 predictors). The models presented here can be used to map *SI* over large areas of forest automatically, determining forest productivity at a much finer spatial resolution than usually possible operational inventories. Future challenges are related to improving the resolution of the raster models, which are currently limited by the spatial sampling of climate and edaphic variables.

Acknowledgements

We gratefully acknowledge the National Forest Inventory Department for supplying the NFI data and the latest version of FMS. We thank Xabier Pons and Miquel Ninyerola (Universitat Autònoma de Barcelona) for their support in acquiring the climate data. This work was partly supported by the ‘National Programme for the Promotion of Talent and Its

Employability' of the Ministry of Economy, Industry, and Competitiveness (Torres-Quevedo program) and by the company 3edata Ingeniería Medioambiental S.L. via a postdoctoral grant (PTQ-13-06378) awarded to Juan Guerra Hernández. This research was initiated during a stay by the second author at the Instituto Superior de Agronomía (University of Lisbon, Portugal), supported by the research group UXAFORES (GI-1837) of the University of Santiago de Compostela and by the BioReDes Strategic Group (ED431E 2018/09) funded by the Galicia Government.

Author Contributions

Conceptualization, JG, SA and JGA; Methodology, JGA; Data preparation, JG, SA, EGF, ADR and JGA; Data Analysis, JGA; Research, JG, EGF, SA, AP and JGA; Resources, VS and JGA; Writing—Original Draft Preparation, JG, SA, EGF, AP, ADR and JGA; Writing—Review & Editing; JG, SA, EGF, AP, ADR and JGA and; Project Administration. VS and JGA.

Funding

This work was partly supported by 'National Programme for the Promotion of Talent and Its Employability' of the Ministry of Economy, Industry, and Competitiveness (Torres-Quevedo program) via a postdoctoral grant (PTQ-13-06378) awarded to Juan Guerra Hernández and for the VIS4FIRE project (RTA 2017-0042-C05-05) of the Spanish Ministry of Economy, Industry, and Competitiveness.

References

Alberdi, I., Cañellas, I., Bombín, R.V., 2017. The Spanish National Forest Inventory: history, development, challenges and perspectives. Brazilian Journal of Forest Research/Pesquisa Florestal Brasileira 37.

Álvarez-Álvarez, P., Khouri, E.A., Cámara-Obregón, A., Castedo-Dorado, F., Barrio-Anta, M., 2011. Effects of foliar nutrients and environmental factors on site productivity in Pinus pinaster Ait. stands in Asturias (NW Spain). Annals of Forest Science 68, 497–509.

Álvarez-González, J.G., Cañellas, I., Alberdi, I., Gadow, K.V., Ruiz-González, A.D., 2014. National Forest Inventory and forest observational studies in Spain: Applications to forest modeling. Forest Ecology and Management 316, 54–64.

Álvarez-González, J.G., Ruiz-González, A.D., Rodríguez-Soalleiro, R., Barrio-Anta, M., 2005. Ecoregional site index models for Pinus pinaster in Galicia (northwestern Spain). Annals of Forest Science 62, 115–127.

Arias-Rodil, M., Crecente-Campo, F., Barrio-Anta, M., Diéguez-Aranda, U., 2015. Evaluation of age-independent methods of estimating site index and predicting

height growth: a case study for maritime pine in Asturias (NW Spain). European journal of forest research 134, 223–233.
Bailey, R.L., Clutter, J.L., 1974. Base-age invariant polymorphic site curves. Forest Science 20, 155–159.
Ballabio, C., Panagos, P., Monatanarella, L., 2016. Mapping topsoil physical properties at European scale using the LUCAS database. Geoderma 261, 110–123. https://doi.org/10.1016/j.geoderma.2015.07.006
Bravo-Oviedo, A., del Río, M., Montero, G., 2007. Geographic variation and parameter assessment in generalized algebraic difference site index modelling. Forest ecology and management 247, 107–119.
Bravo-Oviedo, A., Tome, M., Bravo, F., Montero, G., Del Rio, M., 2008. Dominant height growth equations including site attributes in the generalized algebraic difference approach. Canadian Journal of Forest Research 38, 2348–2358.
Brent, R.P., 1973. Algorithms for Minimization without Derivatives, chap. 4. Prentice-Hall, Englewood Cliffs, NJ.
Burkhart, H.E., Tomé, M., 2012. Modeling forest trees and stands. Springer Science & Business Media.
Campoe, O.C., Munhoz, J.S., Alvares, C.A., Carneiro, R.L., de Mattos, E.M., Ferez, A.P.C., Stape, J.L., 2016. Meteorological seasonality affecting individual tree growth in forest plantations in Brazil. Forest Ecology and Management 380, 149–160.
Castedo-Dorado, F., Diéguez-Aranda, U., Álvarez-González, J.G., 2007. A growth model for Pinus radiata D. Don stands in north-western Spain. Annals of Forest Science 64, 453–465.
Cieszewski, C.J., 2004. GADA derivation of dynamic site equations with polymorphism and variable asymptotes from Richards, Weibull, and other exponential functions. University of Georgia PMRC-TR 5, 2004.
Cieszewski, C.J., 2002. Comparing fixed-and variable-base-age site equations having single versus multiple asymptotes. Forest Science 48, 7–23.
Cieszewski, C.J., Bailey, R.L., 2000. Generalized algebraic difference approach: theory based derivation of dynamic site equations with polymorphism and variable asymptotes. Forest Science 46, 116–126.
Clark, M.L., Clark, D.B., Roberts, D.A., 2004. Small-footprint lidar estimation of sub-canopy elevation and tree height in a tropical rain forest landscape. Remote Sensing of Environment 91, 68–89.
Clutter, J.L., Fortson, J.C., Pienaar, L.V., Brister, G.H., Bailey, R.L., 1983. Timber management: A quantitative approach. John Wiley & Sons, Inc.
Condés, S., García-Robredo, F., 2012. An empirical mixed model to quantify climate influence on the growth of Pinus halepensis Mill. stands in South-Eastern Spain. Forest ecology and management 284, 59–68.
Diéguez-Aranda, U., Alboreca, A.R., Castedo-Dorado, F., González, J.Á., Barrio-Anta, M., Crecente-Campo, F., González, J.G., Pérez-Cruzado, C., Soalleiro, R.R., López-Sánchez, C.A., 2012. Adenda. Herramientas selvícolas para la gestión forestal sostenible en Galicia. Actualización de modelos disponibles a fecha de 29/10/2012.(Available on: https://www.uxafores.com) (accessed on May, 2020).
Diéguez-Aranda, U., Alboreca, A.R., Castedo-Dorado, F., González, J.Á., Barrio-Anta, M., Crecente-Campo, F., González, J.G., Pérez-Cruzado, C., Soalleiro, R.R., López-Sánchez, C.A., 2009. Herramientas selvícolas para la gestión forestal sostenible en Galicia. Xunta de Galicia. Santiago de Compostela. 82.

Diéguez-Aranda, U., Dorado, F.C., González, J.G.Á., Alboreca, A.R., 2006a. Dynamic growth model for Scots pine (Pinus sylvestris L.) plantations in Galicia (north-western Spain). Ecological Modelling 191, 225–242.

Diéguez-Aranda, U., Grandas-Arias, J.A., Álvarez-González, J.G., von Gadow, K., 2006b. Site quality curves for birch stands in north-western Spain. Silva Fennica 40, 631.

Estornell, J., Ruiz, L.A., Velázquez-Martí, B., Hermosilla, T., 2011. Analysis of the factors affecting LiDAR DTM accuracy in a steep shrub area. International Journal of Digital Earth 4, 521–538.

Fernández-Landa, A., Fernández-Moya, J., Tomé, J.L., Algeet-Abarquero, N., Guillén-Climent, M.L., Vallejo, R., Sandoval, V., Marchamalo, M., 2018. High resolution forest inventory of pure and mixed stands at regional level combining National Forest Inventory field plots, Landsat, and low density lidar. International journal of remote sensing 39, 4830–4844.

Friedman, J.H., 1991. Multivariate adaptive regression splines. The annals of statistics 1–67.

Gatziolis, D., Fried, J.S., Monleon, V.S., 2010. Challenges to estimating tree height via LiDAR in closed-canopy forests: A parable from western Oregon. Forest Science 56, 139–155.

Gazol, A., Camarero, J.J., Anderegg, W.R.L., Vicente-Serrano, S.M., 2017. Impacts of droughts on the growth resilience of Northern Hemisphere forests. Global Ecology and Biogeography 26, 166–176.

Gleason, K.E., Bradford, J.B., Bottero, A., D'Amato, A.W., Fraver, S., Palik, B.J., Battaglia, M.A., Iverson, L., Kenefic, L., Kern, C.C., 2017. Competition amplifies drought stress in forests across broad climatic and compositional gradients. Ecosphere 8, e01849.

Gonçalves-Seco, L., González-Ferreiro, E., Diéguez-Aranda, U., Fraga-Bugallo, B., Crecente, R., Miranda, D., 2011. Assessing the attributes of high-density Eucalyptus globulus stands using airborne laser scanner data. International Journal of Remote Sensing 32, 9821–9841.

González, J.G.Á., González, A.D.R., Soalleiro, R.R., Anta, M.B., 2005. Ecoregional site index models for Pinus pinaster in Galicia (northwestern Spain). Annals of Forest Science 62, 115–127.

González-Rodríguez, M.A., Diéguez-Aranda, U., 2020. Exploring the use of learning techniques for relating the site index of radiata pine stands with climate, soil and physiography. Forest Ecology and Management 458, 117803.

Gracia, C.A., Tello, E., Sabaté, S., Bellot, J., 1999. GOTILWA: An Integrated Model of Water Dynamics and Forest Growth, in: Rodà, F., Retana, J., Gracia, C.A., Bellot, J. (Eds.), Ecology of Mediterranean Evergreen Oak Forests. Springer Berlin Heidelberg, Berlin, Heidelberg, pp. 163–179. https://doi.org/10.1007/978-3-642-58618-7_12

Guerra-Hernández, J., Aviles, C., Botequim, B., Jurado-Varela, A., Sandoval, V., Robla-González, E., 2019. Expansión continua del IFN4 de Extremadura y Canarias mediante técnicas LiDAR, in: Teledetección: Hacia Una Visión Global Del Cambio Climático. Valladolid, pp. 467-470.

Guerra-Hernández, J., Tomé, M., González-Ferreiro, E., 2016. Using low density LiDAR data to map Mediterranean forest characteristics by means of an area-based approach and height threshold analysis. Revista de Teledetección 46, 103–117.

Hijmans, R.J., van Etten, J., Cheng, J., Mattiuzzi, M., Sumner, M., Greenberg, J.A., Lamigueiro, O.P., Bevan, A., Racine, E.B., Shortridge, A., 2015. Package 'raster.' R package.

868 Hopkinson, C., Chasmer, L., Hall, R.J., 2008. The uncertainty in conifer plantation growth
869 prediction from multi-temporal lidar datasets. Remote Sensing of Environment 112,
870 1168–1180. https://doi.org/10.1016/j.rse.2007.07.020
871 Huang, S., Yang, Y., Wang, Y., 2003. A critical look at procedures for validating growth
872 and yield models. Modelling forest systems 1.
873 Hyyppä, J., Hyyppä, H., Leckie, D., Gougeon, F., Yu, X., Maltamo, M., 2008. Review of
874 methods of small-footprint airborne laser scanning for extracting forest inventory
875 data in boreal forests. International Journal of Remote Sensing 29, 1339–1366.
876 Institute, S.A.S., 2004. SAS/ETS 9.1 User's Guide. SAS Institute.
877 Isenburg, M., 2020. LAStools—efficient tools for LiDAR processing (Version 200216,
878 academic).
879 Kahriman, A., Sönmez, T., Gadow, K. von, 2018. Site index models for Calabrian pine in
880 the central Mediterranean region of Turkey. Journal of Sustainable Forestry 37,
881 459–474.
882 Kimmins, J.P., Comeau, P.G., Kurz, W., 1990. Modelling the interactions between
883 moisture and nutrients in the control of forest growth. Forest Ecology and
884 Management 30, 361–379.
885 Klos, R.J., Wang, G.G., Bauerle, W.L., Rieck, J.R., 2009. Drought impact on forest growth
886 and mortality in the southeast USA: an analysis using Forest Health and Monitoring
887 data. Ecological Applications 19, 699–708. https://doi.org/10.1890/08-0330.1
888 Korf, V., 1939. A mathematical definition of stand volume growth law. Lesnická práce 18,
889 337–339.
890 Lauer, D.K., Kush, J.S., 2010. Dynamic Site Index Equation for Thinned Stands of Even-
891 Aged Natural Longleaf Pine. Southern Journal of Applied Forestry 34, 28–37.
892 https://doi.org/10.1093/sjaf/34.1.28
893 Liu, Y., El-Kassaby, Y.A., 2018. Evapotranspiration and favorable growing degree-days
894 are key to tree height growth and ecosystem functioning: Meta-analyses of Pacific
895 Northwest historical data. Scientific Reports 8, 8228.
896 https://doi.org/10.1038/s41598-018-26681-1
897 MAGRAMA, 2018. 5th Spanish National Forest Inventory, Ministry of Agriculture, Food
898 and Environment. Ministerio de Agricultura, Alimentación y Medio Ambiente.
899 MAGRAMA, 2012. 4rd Spanish National Forest Inventory, Ministry of Agriculture, Food
900 and Environment. Ministerio de Agricultura, Alimentación y Medio Ambiente.
901 MAGRAMA, 2010. Anuario de Estadística Forestal 2010. Ministerio de Agricultura,
902 Alimentación y Medio Ambiente.
903 Maltamo, M., Næsset, E., Vauhkonen, J., 2014. Forestry applications of airborne laser
904 scanning. Springer.
905 MAPA, 2018. Mapa Forestal de las Especies Productivas del Norte Peninsular. Escala
906 1:25.000. Ministerio de Agricultura,Pesca y Alimentación. Dirección General de
907 Desarrollo Rural, Innovación y Política Forestal.
908 Martínez-Vilalta, J., López, B.C., Adell, N., Badiella, L., NINYEROLA, M., 2008.
909 Twentieth century increase of Scots pine radial growth in NE Spain shows strong
910 climate interactions. Global Change Biology 14, 2868–2881.
911 https://doi.org/10.1111/j.1365-2486.2008.01685.x
912 Milborrow, S., Hastei, T., Tibshirani, R., Miller, A., Lumley, T., 2019. earth: Multivariate
913 Adaptive Regression Splines. R package version 5.1.1. (Available on:
914 https://CRAN.R-project.org/package=earth) (accessed on May, 2020).
915 Monserud, R.A., 1984. Height growth and site index curves for inland Douglas-fir based on
916 stem analysis data and forest habitat type. Forest Science 30, 943–965.
917 Naesset, E., 1997. Estimating timber volume of forest stands using airborne laser scanner
918 data. Remote Sensing of Environment 61, 246–253.

Ninyerola, M., Pons, X., Roure, J.M., 2007. Objective air temperature mapping for the Iberian Peninsula using spatial interpolation and GIS. International Journal of Climatology: A Journal of the Royal Meteorological Society 27, 1231–1242.
Ninyerola, M., Pons, X., Roure, J.M., 2000. A methodological approach of climatological modelling of air temperature and precipitation through GIS techniques. International Journal of Climatology: A Journal of the Royal Meteorological Society 20, 1823–1841.
Noordermeer, L., Bollandsås, O.M., Gobakken, T., Næsset, E., 2018. Direct and indirect site index determination for Norway spruce and Scots pine using bitemporal airborne laser scanner data. Forest Ecology and Management 428, 104–114.
Noordermeer, L., Gobakken, T., Næsset, E., Bollandsås, O.M., 2020. Predicting and mapping site index in operational forest inventories using bitemporal airborne laser scanner data. Forest Ecology and Management 457, 117768. https://doi.org/10.1016/j.foreco.2019.117768
Nunes, L., Patrício, M., Tomé, J., Tomé, M., 2011. Modeling dominant height growth of maritime pine in Portugal using GADA methodology with parameters depending on soil and climate variables. Annals of Forest Science 68, 311–323.
Panagos, P., Liedekerke, M. [Van, Jones, A., Montanarella, L., 2012. European Soil Data Centre: Response to European policy support and public data requirements. Land Use Policy 29, 329–338. https://doi.org/10.1016/j.landusepol.2011.07.003
Pascual, A., Guerra-Hernández, J., Cosenza, D.N., Sandoval, V., 2020. The Role of Improved Ground Positioning and Forest Structural Complexity When Performing Forest Inventory Using Airborne Laser Scanning. Remote Sensing 12, 413.
Pons, X., Ninyerola, M., 2008. Mapping a topographic global solar radiation model implemented in a GIS and refined with ground data. International Journal of Climatology: A Journal of the Royal Meteorological Society 28, 1821–1834.
R Core Team, 2020. R: A language and environment for statistical computing (Version 3.6. 1)[Computer software]. Vienna, Austria: R Foundation for Statistical Computing.
Raber, G.T., Jensen, J.R., Schill, S.R., Schuckman, K., 2002. Creation of digital terrain models using an adaptive lidar vegetation point removal process. Photogrammetric engineering and remote sensing 68, 1307–1314.
Rennolls, K., 1978. Top Height; Its definition and estimation. The Commonwealth Forestry Review 215–219.
Rivas-Martinez, S., 2008. Synoptical worldwide bioclimatic classification system. Available on line at http://www. globalbioclimatics. org/book/claves. htm. (Accessed on May, 2020).
Rodríguez-Soalleiro, R., 1995. Crecimiento y producción de masas forestales de pinus pinaster ait. en Galicia. Alternativas silvícolas posibles. Universidad Politécnica de Madrid.
Roussel, J.-R., Caspersen, J., Béland, M., Thomas, S., Achim, A., 2017. Removing bias from LiDAR-based estimates of canopy height: Accounting for the effects of pulse density and footprint size. Remote Sensing of Environment 198, 1–16.
Scolforo, H.F., McTague, J.P., Burkhart, H., Roise, J., Alvares, C.A., Stape, J.L., 2020. Site index estimation for clonal eucalypt plantations in Brazil: A modeling approach refined by environmental variables. Forest Ecology and Management 466, 118079.
Scolforo, H.F., McTague, J.P., Burkhart, H., Roise, J., Campoe, O., Stape, J.L., 2019. Eucalyptus growth and yield system: Linking individual-tree and stand-level growth models in clonal Eucalypt plantations in Brazil. Forest Ecology and Management 432, 1–16.
Scolforo, H.F., Neto, F. de C., Scolforo, J.R.S., Burkhart, H., McTague, J.P., Raimundo, M.R., Loos, R.A., Fonseca, S. da, Sartório, R.C., 2016. Modeling dominant height

growth of eucalyptus plantations with parameters conditioned to climatic variations. Forest Ecology and Management 380, 182–195. https://doi.org/10.1016/j.foreco.2016.09.001
Scolforo, J.R.S., Maestri, R., Ferraz Filho, A.C., de Mello, J.M., de Oliveira, A.D., de Assis, A.L., 2013. Dominant height model for site classification of Eucalyptus grandis incorporating climatic variables. International Journal of Forestry Research 2013.
Seki, M., Sakici, O.E., 2017. Dominant height growth and dynamic site index models for Crimean pine in the Kastamonu–Taşköprü region of Turkey. Canadian Journal of Forest Research 47, 1441–1449. https://doi.org/10.1139/cjfr-2017-0131
Skovsgaard, J.P., Vanclay, J.K., 2008. Forest site productivity: a review of the evolution of dendrometric concepts for even-aged stands. Forestry: An International Journal of Forest Research 81, 13–31.
Socha, J., Hawryło, P., Stereńczak, K., Miścicki, S., Tymińska-Czabańska, L., Młocek, W., Gruba, P., 2020. Assessing the sensitivity of site index models developed using bi-temporal airborne laser scanning data to different top height estimates and grid cell sizes. International Journal of Applied Earth Observation and Geoinformation 91, 102129. https://doi.org/10.1016/j.jag.2020.102129
Socha, J., Pierzchalski, M., Bałazy, R., Ciesielski, M., 2017. Modelling top height growth and site index using repeated laser scanning data. Forest Ecology and Management 406, 307–317. https://doi.org/10.1016/j.foreco.2017.09.039
Solberg, S., Kvaalen, H., Puliti, S., 2019. Age-independent site index mapping with repeated single-tree airborne laser scanning. Scandinavian Journal of Forest Research 34, 763–770.
Thornthwaite, C.W., 1933. The climates of the earth. Geographical Review 23, 433–440.
Tomé, J., Tomé, M., Barreiro, S., Paulo, J.A., 2006. Age-independent difference equations for modelling tree and stand growth. Canadian Journal of Forest Research 36, 1621–1630.
Tompalski, P., Coops, N.C., Marshall, P.L., White, J.C., Wulder, M.A., Bailey, T., 2018. Combining multi-date airborne laser scanning and digital aerial photogrammetric data for forest growth and yield modelling. Remote Sensing 10, 347.
Tompalski, P., Coops, N.C., White, J.C., Wulder, M.A., 2016. Enhancing forest growth and yield predictions with airborne laser scanning data: Increasing spatial detail and optimizing yield curve selection through template matching. Forests 7, 255.
Tompalski, P., Coops, N.C., White, J.C., Wulder, M.A., 2015. Augmenting site index estimation with airborne laser scanning data. Forest Science 61, 861–873.
Tompalski, P., Rakofsky, J., Coops, N.C., White, J.C., Graham, A.N., Rosychuk, K., 2019. Challenges of Multi-Temporal and Multi-Sensor Forest Growth Analyses in a Highly Disturbed Boreal Mixedwood Forests. Remote Sensing 11, 2102.
Valbuena, R., Mauro, F., Arjonilla, F.J., Manzanera, J.A., 2011. Comparing airborne laser scanning-imagery fusion methods based on geometric accuracy in forested areas. Remote Sensing of Environment 115, 1942–1954.
Vanclay, J.K., Skovsgaard, J.P., 1997. Evaluating forest growth models. Ecological Modelling 98, 1–12.
Vargas-Larreta, B., Aguirre-Calderón, O.A., Corral-Rivas, J.J., Crecente-Campo, F., Diéguez-Aranda, U., 2013. A dominant height growth and site index model for Pinus pseudostrobus Lindl. in northeastern Mexico. Agrociencia 47, 91–106.
Véga, C., St-Onge, B., 2008. Height growth reconstruction of a boreal forest canopy over a period of 58 years using a combination of photogrammetric and lidar models. Remote Sensing of Environment 112, 1784–1794.

Vicente-Serrano, S.M., Camarero, J.J., Azorin-Molina, C., 2014. Diverse responses of forest growth to drought time-scales in the Northern Hemisphere. Global Ecology and Biogeography 23, 1019–1030. https://doi.org/10.1111/geb.12183

Von Bertalanffy, L., 1957. Quantitative laws in metabolism and growth. The quarterly review of biology 32, 217–231.

Weiskittel, A.R., Hann, D.W., Kershaw Jr, J.A., Vanclay, J.K., 2011. Forest growth and yield modeling. John Wiley & Sons.

Wickramasinghe, A., 1988. Modeling Tree Growth Potential Based on Effective Evapotranspiration. Forest Science 34, 864–881. https://doi.org/10.1093/forestscience/34.4.864

Yu, X., Hyyppä, J., Hyyppä, H., Maltamo, M., 2004. Effects of flight altitude on tree height estimation using airborne laser scanning. Proceedings of the Laser Scanners for Forest and Landscape Assessment–Instruments, Processing Methods and Applications 02–06.

Yu, X., Hyyppä, J., Kukko, A., Maltamo, M., Kaartinen, H., 2006. Change detection techniques for canopy height growth measurements using airborne laser scanner data. Photogrammetric Engineering & Remote Sensing 72, 1339–1348.